IJMMM International Journal of Minerals, Metallurgy and Materials 矿物冶金与材料学报（英文版）

Effect of dissolved-oxygen on the flotation behavior of pyrite at high altitude area

Yan Miao, Guangke Ye, and Guofan Zhang

Cite this article as:
Yan Miao, Guangke Ye, and Guofan Zhang, Effect of dissolved-oxygen on the flotation behavior of pyrite at high altitude area, *Int. J. Miner. Metall. Mater.*, 31(2024), No. 10, pp. 2148-2158. https://doi.org/10.1007/s12613-023-2784-5

View the article online at SpringerLink or IJMMM Webpage.

INTERNATIONAL JOURNAL OF
Minerals, Metallurgy and Materials

Volume 31, Number 10, October 2024
Page 2148

Research Article https://doi.org/10.1007/s12613-023-2784-5

Effect of dissolved-oxygen on the flotation behavior of pyrite at high altitude area

Yan Miao, Guangke Ye, and Guofan Zhang✉

School of Minerals Processing and Bio-engineering, Central South University, Changsha 410083, China
(Received: 27 July 2023; revised: 4 October 2023; accepted: 9 November 2023)

Abstract: With the continuous development of mineral resources to high altitude areas, the study of sulfide ore flotation in unconventional systems has been emphasized. There is a consensus that moderate oxidation of sulfide ore is beneficial to flotation, but the specific suitable dissolved oxygen value is inconclusive, and there are few studies on sulfide ore flotation under low dissolved oxygen environment at high altitude. In this paper, we designed and assembled an atmosphere simulation flotation equipment to simulate the flotation of pyrite at high altitude by controlling the partial pressure of N_2/O_2 and dissolved oxygen under atmospheric conditions. X-ray photoelectron spectroscopy (XPS), atomic force microscope (AFM), Fourier transform infrared spectrometer (FT-IR), UV-vis spectrophotometer, zeta potential, and contact angle measurements were used to reveal the effects of surface oxidation and agent adsorption on pyrite at high altitude (4600 m dissolved oxygen (DO) = 4.0 mg/L). The results of pure mineral flotation indicated that the high altitude and low dissolved oxygen environment is favorable for pyrite flotation. Contact angle measurements and XPS analysis showed that the high altitude atmosphere slows down the oxidation of pyrite surface, facilitates S_n^{2-}/S^0 production and enhances surface hydrophobicity. Electrochemical calculations and zeta potential analysis showed that the influence of atmosphere on the form of pyrite adsorption is small, and the different atmospheric conditions are consistent with dixanthogen electrochemical adsorption, with lower Zeta potential under high altitude atmosphere and significant potential shift after sodium isobutyl xanthate (SIBX) adsorption. The results of FT-IR, UV-vis, and AFM analysis showed that SIBX adsorbed more on the surface of pyrite under high altitude atmosphere and adsorbed on the surface in a mesh structure composed of column/block. The results of the experimental study revealed the reasons for the easy flotation of sulfide ores at high altitude with less collector dosage, and confirmed that the combined DO–pH regulation is beneficial to achieve more efficient flotation of pyrite.

Keywords: high altitude; dissolved-oxygen; pyrite; flotation; oxidation

1. Introduction

High altitude mines are characterized by low pressure and oxygen gas environment, dry climate, fragile environment, inconvenient transportation, and so on. The flotation has a wide range of applications and high efficiency, so that sulfide mines are still widely used in high altitude. Compared with conventional systems, the dissolved oxygen (DO) in the water is lower due to the low pressure and oxygen environment at high altitude, and the flotation effect may also be different. The situation affects the surface oxidation of pyrite and the electrochemical reaction of the agent and mineral. The mechanism of influence on flotation of sulfide minerals in this environment is lack of systematic research.

Many scholars have studied the effect of dissolved oxygen on the surface oxidation of pyrite, and its floatability is related to the generation of hydrophobic substances (S_n^{2-}/S^0) on the surface. The oxidation process of elemental sulfur on the surface of pyrite has been studied by some authors, where S^0 is produced on the surface only in the presence of dissolved oxygen, and the amount of S^0 reaches a maximum when DO is 20wt% of its saturation value in the slurry [1–2]. Sulfur oxidation is also closely related to the pulp pH, where a decrease in pH accelerates the dissolution of metal ions, which favors S^0 generation and increases floatability. If moderate oxygen oxidation, it is beneficial to achieve collector-free flotation of sulfide ore or reduce the consumption of collector. If excessive oxidation occurs, hydrophilic sulfur oxides (such as $S_2O_3^{2-}$ and SO_4^{2-}) are produced, which can inhibit its flotation [3–5]. There are scholars performed the separation of chalcopyrite and pyrite by adding O_3 and H_2O_2 [4,6–7]. The results showed that the floatability of chalcopyrite decreased significantly after oxidation, while H_2O_2 exhibited a higher separation selectivity than O_3 oxidation [4–5]. The XPS results also showed that the decrease in floatability was related to the generation of hydrophilic substances such as CuO, $Cu(OH)_2$, FeOOH, and $Fe_2(SO_4)_3$. The oxidation effect on the surface of the sulfide ore also determines the adsorption effect of the agent. Pyrite oxidized by H_2O_2 or exposed to air for a long time will hinder the adsorption of the collector and significantly reduce its floatability, which may be related to the FeOOH or $Fe(OH)_3$ on the surface of pyrite

✉ Corresponding author: Guofan Zhang E-mail: moonwalker00@163.com

[8–11]. Pyrite electrochemical studies have shown that the nitrogen atmosphere leads to a low slurry potential, which inhibits the formation of oxidation products and facilitates their flotation [12]. However, low potential is also detrimental to the adsorption of the collector agent, which may also have an effect on its flotation effect [13–15]. Martin *et al*. [12] conducted flotation tests on pyrite by using nitrogen and the results showed that the slurry still had sufficient oxygen mass transfer. Moreover, nitrogen is beneficial for pyrite flotation by reducing the formation of hydroxyl groups in the slurry [16]. Much research has been carried out on the effect of dissolved oxygen on sulfide ore flotation, however, the optimal DO for sulfide ore flotation has not been clarified, and the relationship between the effect of the altitude–DO on the flotation effect of sulfide ore has not been effectively established.

An atmospheric flotation plant was designed and assembled under atmospheric pressure conditions. The relative O_2/N_2 ratio was adjusted to simulate different altitude atmospheres based on the dissolved oxygen in water at different altitudes. On this basis, the effect of different altitude atmospheres on the flotation effect of pyrite was investigated. Contact angle measurements, X-ray photoelectron spectroscopy (XPS), Fourier transform infrared spectrometer (FT-IR), UV-vis spectrophotometer, atomic force microscope (AFM), and electrochemical analysis were used to reveal the surface property changes and agent adsorption behavior of pyrite. The correlation between altitude and pyrite flotation was established, further expanding the environment for the use of sulfide ore flotation theory. The results of the experimental study provide a theoretical basis for sulfide ore flotation in high altitude areas.

2. Experimental

2.1. Materials

Pyrite from a metamorphic mine in Hubei, China, and the chemical analysis is shown in Table 1. The purity is 97.3%. The test sample was crushed by ceramic crushing, ceramic grinding and dry sieving to 38–74 μm, sealed by sealed bag, dried by silica gel ball, and stored in refrigerator. The pyrite crystals were analyzed by X-ray diffraction (XRD). Fig.1 shows the main peaks of the pure mineral are obvious and basically free of spurious peaks, with a single mineral crystal and high purity.

Table 1. Chemical multi-element analysis of pyrite wt%

TFe	TS	SiO_2	Al_2O_3	MgO
45.41	51.90	0.65	0.47	0.54

The sulfide ore collector sodium isobutyl xanthate (SIBX, AR) was purchased from Hunan Minzhu Mineral Processing Chemical Co., Ltd. The methyl isobutyl carbinol (MIBC, AR) was purchased from Jiangxi Tianzhuo Flotation Reagent Co. The adjusting agents CaO and NaOH (AR) were purchased from Xilong Chemical Co. Ultra-pure water (R > 18.0 MΩ/cm) was used for all tests, and nitrogen was used to drive oxygen before the test (DO < 0.3 mg/L).

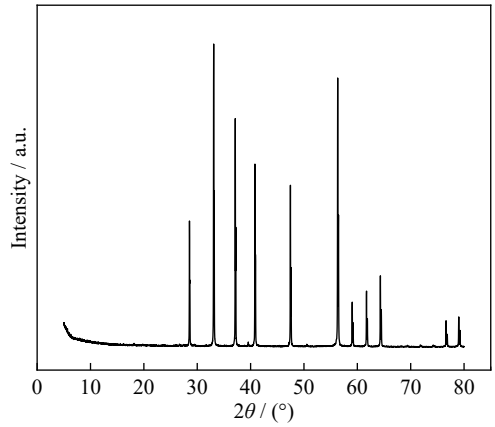

Fig. 1. XRD pattern of pyrite.

2.2. High altitude–DO

The atmosphere consists of 78.09vol% nitrogen, 20.95vol% oxygen, and 0.96vol% carbon dioxide and ozone. The atmospheric pressure is equal to the sum of the partial pressure of oxygen and the partial pressure of all other gases. Based on the literature [17], it is known that the equation of isothermal atmospheric pressure versus altitude (Laplace's formula for pressure height) is shown as Eq. (1), and Eq. (2) is obtained by conversion at 25°C. The oxygen partial pressure is calculated as shown in Eqs. (3)–(4).

$$\ln P = -Z \times g/(R_d \times T) + \ln P_0 \quad (1)$$

$$\ln P = -0.03 \times (Z/10000)^3 - 0.126 \times (Z/10000)^2 - 1.19 \times (Z/10000) + 4.62 \quad (2)$$

$$P_{O_2} = P \times 20.95\% \quad (3)$$

$$P_{O_2} = K \times X_{O_2} \quad (4)$$

where Z is the altitude, P is the corresponding altitude pressure, P_0 is the sea level pressure, T is the thermodynamic temperature, g is the acceleration of gravity, R_d is the ideal gas constant, K is the Henry coefficient, and X_{O_2} is the molar fraction of oxygen in water.

Henry's law shows that the solubility of a gas in a liquid at a given temperature is proportional to the equilibrium partial pressure of that gas, and the Henry's coefficient (K) depends on temperature, pressure, and the nature of the solute and solvent [18–19]. The dissolved oxygen (DO) parameters corresponding to different altitudes in Table 2 are the measured values in the vacuum test chamber, which are close to the calculated theoretical values and serve as reference values for dissolved oxygen conditions at high altitudes.

According to the difference of mountain type and scale, the altitude was divided into high mountain areas >3000 m, mountain or hilly areas from 1000 to 3000 m, and low mountain hilly or plain areas <1000 m. To study the effect of DO on sulfide ore flotation at high altitude, the oxygen partial pressure was adjusted by changing the atmosphere composition under atmospheric pressure conditions, and high altitude atmosphere composition was simulated with dissolved oxygen as the characterization parameter. As shown in Table 2,

Table 2. Relationship between altitude and dissolved oxygen

Altitude / m	Air pressure / kPa	O_2 pressure / kPa	O_2 concentration / vol%	DO / (mg·L^{-1})
0	101.3	21.0	20.9	8.17
1000	89.9	18.7	18.6	7.15
2000	79.5	16.5	16.4	6.21
3000	70.3	14.6	14.5	5.35
4000	62.1	12.9	12.8	4.56
5000	54.9	11.4	11.3	3.84

Note: Oxygen concentration relative to the percentage value at atmospheric pressure and dissolved oxygen temperature condition of 25°C.

the dissolved oxygen parameter in water under high altitude 4600 m environment is 4.0 mg/L, whereas it is 6.0 and 8.1 mg/L under middle altitude 1800 m environment and low altitude (63 m in Changsha) environment, respectively.

2.3. Equipment and process

The connection diagram of the test equipment is shown in Fig. 2, including gas cylinder, gas mixing chamber, Hallimount tube, and magnetic stirring device. The flotation test is carried out in Hallimount tube with an effective volume of 90 mL, a built-in ceramic microporous foam plate, a miniature magnetic rotor, and a speed setting of 1500 r/min. The test gas supply is purchased from Changsha Xinxiang Gas & Chemical Co. The gas is feed into the tube, and the gas flow rate is controlled at 175–200 mL/min. The external atmosphere has no influence on the internal flotation system.

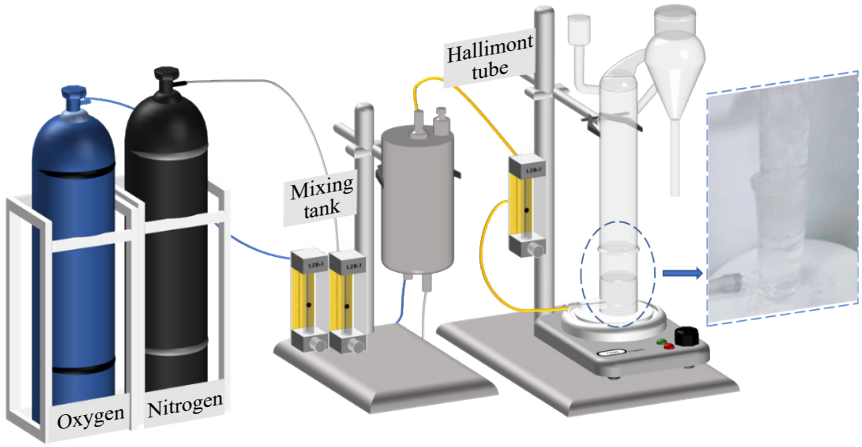

Fig. 2. Diagram of the self-made microflotation equipment.

In the condition of atmospheric pressure and room temperature of 25°C, the control of DO in water is mainly regulated by adjusting the partial pressure of oxygen in the atmosphere, and the purpose of simulating high altitude atmosphere is achieved by controlling the concentration of mixed gas oxygen under the condition of constant total pressure in the gas mixing chamber. In order to determine the effect of mixed gas oxygen concentration and inflation time on the dissolved oxygen content in water, DO was measured dynamically with oxygen concentration meter model BH-4M, dissolved oxygen meter model JPSJ-606L, and electrode model DO-958-L. The DO value was measured under the inflation volume of 175 mL/min and stirring speed of 1500 r/min, and the results are shown in Fig. 3. The oxygen concentration was 20.9vol% in the atmospheric environment of atmospheric pressure and low altitude (63 m in Changsha), and the DO value in water was stabilized at about 8.1 mg/L when it was inflated for 8 min. When the oxygen concentration of the gas mixture is (16 ± 0.6)vol%, the DO value in water can be controlled at (4.0 ± 0.2) mg/L when inflated for 4 min, which is close to the dissolved oxygen value in water at 4600 m altitude, and this atmosphere condition under atmospheric pressure can basically achieve the purpose of simulating high altitude atmosphere.

Oxygen was driven by nitrogen for 6 min before the test, and then the different altitude atmosphere was adjusted to in-

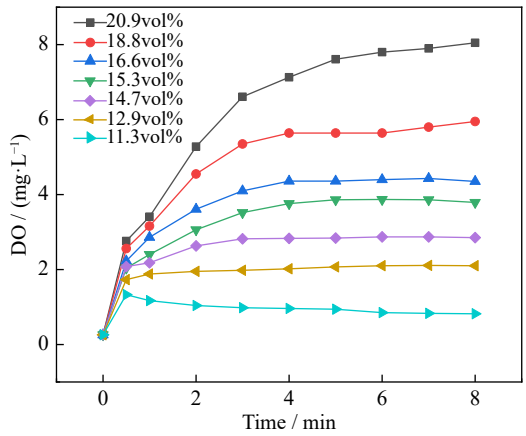

Fig. 3. Relationship between atmosphere and dissolved oxygen.

flate for 8 min until the DO value was stable. The flotation flowsheet is shown in Fig. 4. After adding 2 g of pure minerals and stirring for 8 min, pH regulator, collector agent, and 4.5 μL MIBC were added in tube as frother agent.

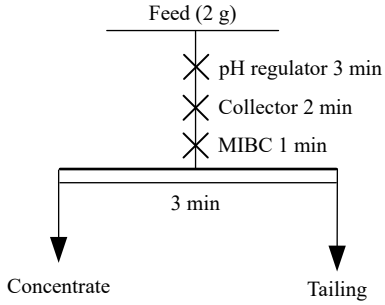

Fig. 4. Single flotation flowsheet.

2.4. Analysis

(1) XPS analysis.

Model: Thermo Scientific Kα, X-ray source: Al Kα rays ($h\nu$ = 1486.6 eV). After the powder sample was pressed and attached to the sample tray, the sample was placed into the sample chamber of the instrument, and the sample was fed into the analysis chamber when the pressure in the sample chamber was less than 2.0×10^{-5} Pa, with a spot size of 400 μm, an operating voltage of 12 kV, and a filament current of 6 mA. The full-spectrum scan fluence energy was 150 eV in steps of 1 eV. The narrow-spectrum scan fluence energy was 50 eV in steps of 0.1 eV, and at least 5 cycles of signal accumulation were performed for the narrow spectrum.

(2) FT-IR analysis.

Model: Shimadzu Instruments IRAffinity, scan range 400–4000 cm^{-1}, resolution: 0.5 cm^{-1}, 30° incidence Michelson interferometer, diffuse reflectance measurement. Pyrite particles were treated with reagents and gases in a vacuum chamber, and then the samples were dried at low temperature in a vacuum drying chamber.

(3) UV-vis analysis.

Model: Unico UV2100, using UV spectrophotometry to analyze the concentration of pharmaceuticals in solution. The absorbance of the solution was measured at the characteristic absorption wavelength (the characteristic absorption wavelength of SIBX is 301 nm), and the absorbance standard curve of the agent was made. The sample solution was centrifuged for 10 min using a high-speed centrifuge (10000 r/min), and the clear solution was placed on a cuvette to measure the absorbance at the characteristic absorption wavelength, and the concentration of the agent in the slurry was calculated with reference to the standard curve.

(4) Zeta analysis.

Model: Mal ZEN3600/nanoZS90, the zeta potential measurements were performed under different atmospheres. A 100 mg sample of pyrite was added to 50 mL of 1×10^{-3} mol/L KCl solution and stirred for 5 min, settled for 5 min, and then the suspension sample was taken by syringe for analysis. The pH of the suspension was adjusted using 0.10 mol/L NaOH and HCl at the same time as the measurements. The average of the three measurements for each pH unit was calculated and given.

(5) AFM analysis.

Model: Nanoscope V, Bruker, the tests were performed in Tapping-mode with a single-crystal silicon probe of RTESP-300 model with an imaging resonance frequency of 286 kHz, an elasticity factor of 40 N/m, a scanning frequency of 2 Hz, and a scanning range of 3 μm × 3 μm. The AFM images were represented by different gray levels are indicated, with light colors being high and dark colors being low. All AFM images were collected using Nanoscope analysis software and Flattened to prevent image distortion. Pure mineral crystals were abraded with 2000, 5000, and 8000 mesh sandpaper and polished with 2.5, 1, and 0.5 μm diamond suspensions, and the samples were stored in anhydrous ethanol. The samples were ultrasonically cleaned and blown dry with nitrogen before use, and the treated samples were dried in a vacuum drying oven at low temperature before measurement.

(6) Contact angle test.

Model: Chengde Dingsheng Testing Machine and Testing Equipment Co., Ltd JY-82C, water droplet 0.016 mL/d. The samples were pressed and fixed on a ϕ25 mm mold. The samples were polished with 2000, 3000, and 5000 mesh sandpaper before the test, and then treated with reagents and gases in a vacuum glove box according to the experimental design. The treated samples were dried in a vacuum drying oven at low temperature before contact angle measurement.

3. Results and discussion

3.1. Altitude–pH flotation test

The pH value of slurry was adjusted to 8.0–8.5 with NaOH, and the pyrite collector agent dosage conditions were tested at low altitude, the test results are shown in Fig. 5. The recovery of pyrite was 92.0% when the SIBX dosage at 7.5×10^{-5} mol/L, and the pyrite recovery tended to be stable with the increase of agent dosage. Under the condition of NaOH as pH regulator and 7.5×10^{-5} mol/L SIBX as collector agent, the pH value condition tests were performed at different altitude conditions (Fig. 6).

The pH value has obvious influence on the flotation effect

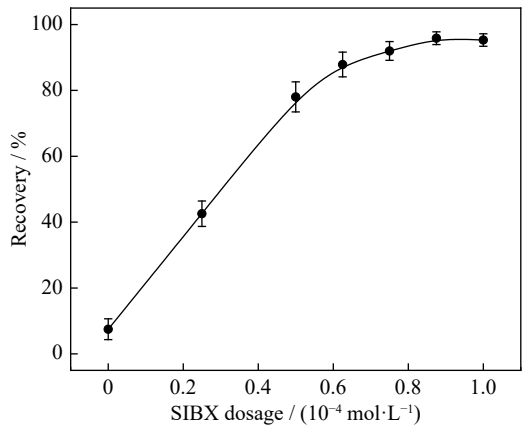

Fig. 5. Relationship between recovery of pyrite and SIBX dosage at low altitude.

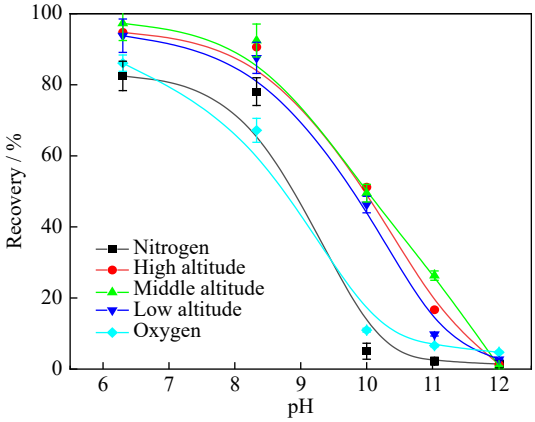

Fig. 6. Recovery of pyrite at different altitude with pH as function.

of pyrite, and the experimental results are the same as the literature [2]. The recovery of pyrite is greater than 80% at pH < 8.0, and pyrite is significantly inhibited at pH > 10.0. The flotation effect of pyrite in high altitude is better than that in low altitude environment, and the DO value in Fig. 3 is slightly lower than that in low altitude. This is resulted from weak alkaline condition would promote pyrite surface oxidation and Fe^{2+} diffusion in solution [20–21]. In addition, the frother was more favorable to the formation of bubbles, and the stability can be improved [22–23]. Based on the small difference between the weakly alkaline and acidic conditions, the condition of pH = 8.0–8.5 was selected for the subsequent test.

3.2. Altitude–SIBX dosage flotation test

The SIBX dosage condition tests were performed at different altitude conditions when the pH = 8.0–8.5.

As shown in Fig. 7, 7.5×10^{-5} mol/L SIBX was the best dosage in different altitude conditions, and the recovery of pyrite was limited by continuing to increase the SIBX dosage. The recovery rate at high altitude is higher than other groups in different agent dosage. Under the same flotation index, high altitude atmosphere can reduce the dosage appropriately.

Pyrite flotation requires moderate oxidation, and the low potential value of slurry is not conducive to electrochemical

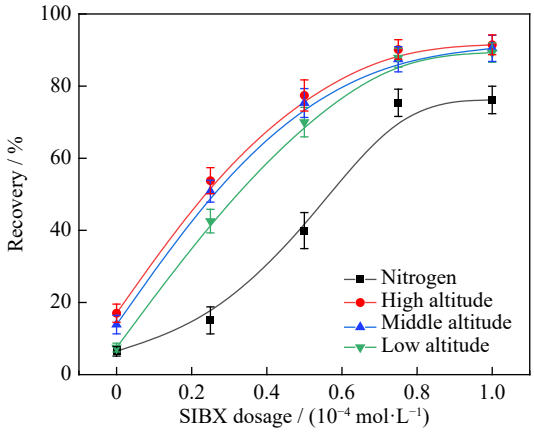

Fig. 7. Recovery of pyrite at different altitude with SIBX dosage as function.

adsorption of the collector agent on the surface of pyrite, which affects its flotation recovery effect. Excessive oxidation of pyrite surface will produce a large number of hydroxyl iron compounds on the surface, which is also detrimental to the flotation recovery [9–10]. Moreover, the effect of surface oxidation of pyrite on the adsorption at high altitude needs to be studied in more depth. The theory of moderate oxidation of pyrite at high altitude can be analyzed from surface sulfur oxidation theory and electrochemical adsorption theory of pyrite.

3.3. Mechanism analysis

The results of the flotation tests all indicate that the low DO at high altitude is favorable for pyrite flotation compared to the low altitude environment. This work focuses on the effect of oxidation on the surface of sulfide minerals and adsorption of chemicals on the hydrophobicity of minerals at high altitude. XPS, FT-IR, AFM, and other microscopic were used to reveal the effect of low DO at high altitude on the surface properties of pyrite, and contact angle macroscopic measurements was used to investigate the changes of its hydrophobicity.

3.3.1. Contact angle analysis

In the flotation process, the hydrophilicity/hydrophobicity of the mineral surface determines the floatability of the mineral, and the contact angle can effectively measure the contact angle magnitude at the interface of solid, liquid, and gas phases on the mineral surface, thus visually reflecting the wettability of the mineral surface. In order to study the effect of different altitude environments and collector agents on the wettability of pyrite, the contact angle of pyrite under different conditions was measured by the suspended drop method.

As shown in Fig. 8, the pyrite shows stronger hydrophobicity at high altitude conditions, which is favorable for the flotation process. This phenomenon may be due to the moderate DO in the high altitude waters prompting more hydrophobic monomeric sulfur production on the surface of pyrite. At low altitude, the DO content in the water increases, resulting in deeper oxidation of the pyrite surface and more hydrophilic SO_4^{2-} and hydroxylated iron, thus reducing the contact angle of pyrite. Different altitude conditions affect the oxidation of pyrite surface, which has an impact on wettability.

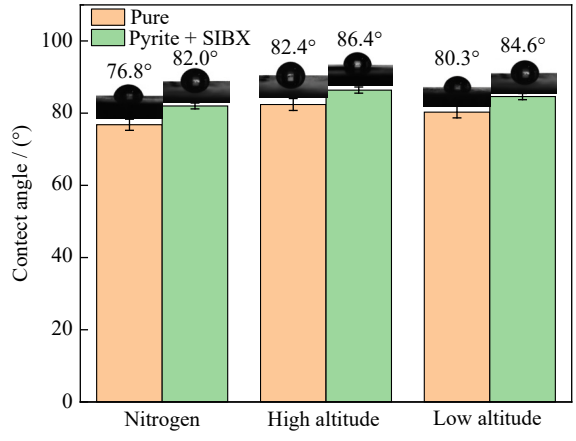

Fig. 8. Contact angle of pyrite at different altitudes.

The contact angle measurement tests show that the wettability of pyrite at high altitude conditions is better than that at low altitude conditions.

3.3.2. XPS analysis

XPS detection was used to study the changes in the chemical valence and atomic concentrations of S and Fe elements on the surface of pyrite under different elevation atmosphere conditions. Fig. 9 shows the XPS spectra of S 2p and Fe 2p and the atomic concentrations of S and Fe components. By fitting S 2p and Fe 2p to the split peaks, it can be observed from Fig. 9(a)–(c) that there is no obvious change in the species of S components on the surface of pyrite under different altitude conditions, mainly the S^{2-} peak corresponds to the presence of sulfur defect sites on the surface, the S_2^{2-} peak corresponds to Fe in the bulk phase of Fe[II]–S_2, and the S_n^{2-}/S^0 peaks correspond to sulfur monomers, iron-deficient sulfides, and polysulfides on the surface of pyrite. When further oxidation of S_n^{2-}/S^0 to higher valence soluble SO_4^{2-} salts is carried out in solution, this affects the total sulfur content of the pyrite surface [24].

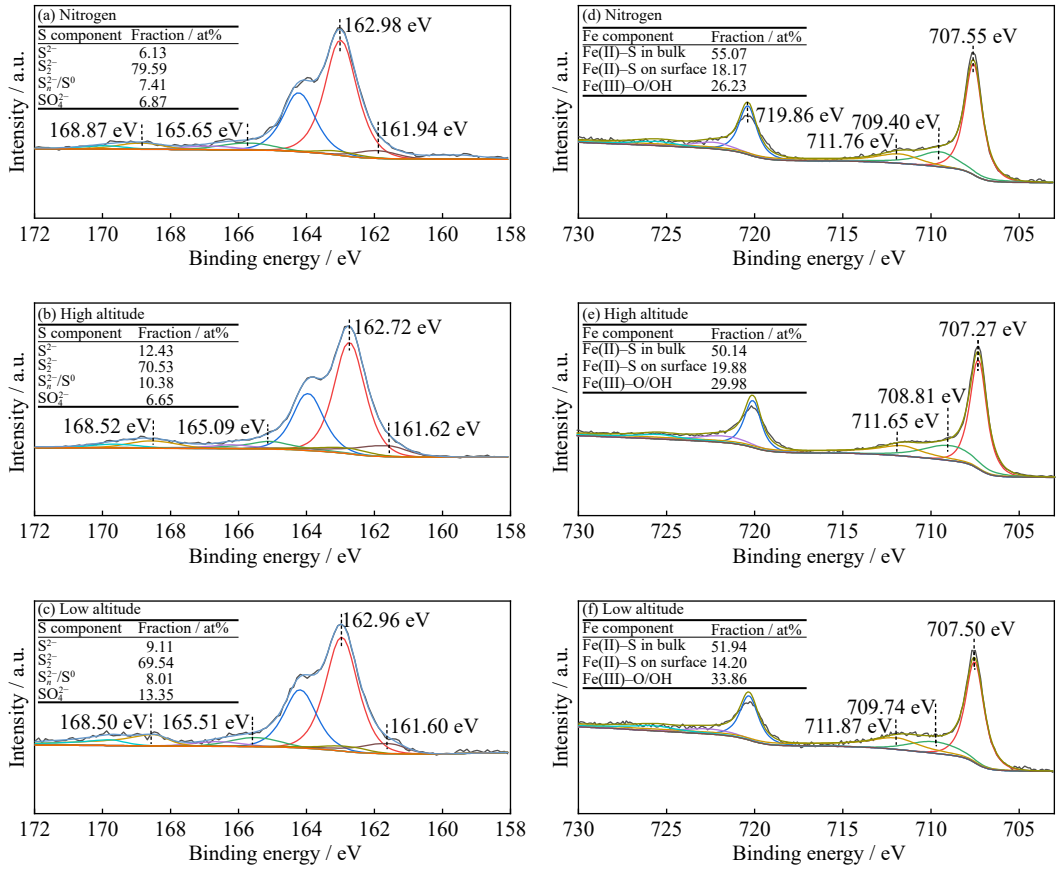

Fig. 9. XPS spectra of (a–c) S 2p and (d–f) Fe 2p of pyrite at nitrogen, high altitude, and low altitude.

As shown in Fig. 9(a)–(c), compared with the nitrogen condition, the oxidation of pyrite occurred under high altitude conditions due to the increase of DO content in the slurry and the intense oxygen mass transfer behavior on the surface of pyrite, which increased the relative content of S^{2-} on the surface from 6.13% to 12.43%. At the same time, according to the "thiosulfate" mechanism followed by pyrite oxidation under alkaline conditions, water molecules reacted at the anode site of pyrite and sulfur atoms lost electrons to be oxidized to $S_2O_3^{2-}$, resulting in an increase in the relative content of S_n^{2-}/S^0 from 7.41% to 10.38%. As the altitude decreases to lower elevations, the relative content of defective sulfur and S_n^{2-}/S^0 on the surface of pyrite decreases to 9.11% and 8.01%, respectively, while the content of SO_4^{2-} increases from 6.65% to 13.35%. As the DO content in the slurry further increased with decreasing elevation, the intermediate valence sulfur oxides on the surface of pyrite were further oxidized to the higher valence SO_4^{2-}. This indicates an increase in sulfur oxidation on the pyrite surface, which in turn makes the pyrite less hydrophobic.

As shown in Fig. 9(d)–(f), the main peak at 707.55 eV corresponds to the fully coordinated low spin Fe^{2+} site in the pyrite lattice, and the peak at 709.40 eV can be interpreted as the surface iron atom bound to sulfur (Fe(II)–S) [25–26]. The shift of Fe(III)–S binding energy under different elevation conditions may be due to the charging effect. The peak of the binding energy located at 711.76 eV is then caused by Fe(III)–O/OH [27–28]. Combined with Fig. 9(e)–(f), it can be observed that the relative concentration of Fe(III)–O/OH gradually increases with decreasing altitude. The DO content in the slurry gradually increases with decreasing altitude, which makes the oxidation on the surface of pyrite increase significantly, further making Fe(III)–O/OH the main component on the surface of pyrite [4]. As the hydrophilic Fe(III)–O/OH covered the surface of pyrite in large amount, on the one hand, it made the surface of pyrite more hydro-

philic; on the other hand, compared with Fe(II)–S, Fe(III)–O/OH showed much weaker interaction with pyrite, which greatly hindered the adsorption of SIBX on the surface of pyrite.

3.3.3. Electrochemical analysis

In order to understand the adsorption form of SIBX at different altitude, the pH and oxidation-reduction potential (ORP) values were monitored during the altitude–pH flotation test. pH meter model is INESA PHS-3E, equipped with E-201-C electrode. ORP potential meter model is INESA YHBJ-262, equipped with 501 ORP electrode, reference electrode was Ag/AgCl, external reference solution was 3 mol/L KCl solution, standard electrode potential E_0 = 0.2224 V, and the standard potential (E vs. SHE) is converted using Eq. (5).

$$E \text{ vs. SHE} = E \text{ vs. Ag/AgCl} + 0.2224 \quad (5)$$

In the pyrite–SIBX flotation system, a redox reaction occurs on the surface of the pyrite to produce dixanthogen (X_2), which is the main hydrophobic substance that causes the pyrite to be floatable, with the following Eqs.:

$$1/2O_2 + H_2O + 2[X^-] = X_2 + 2OH^- \quad (6)$$

$$\text{Cathodic reaction}: \ 1/2O_2 + H_2O + 2e = 2OH^- \quad (7)$$

$$\text{Anodic reaction}: \ 2[X^-] = X_2 + 2e \quad (8)$$

When $E_0 = -0.127$ V and $[X^-] = 7.5 \times 10^{-5}$ mol/L,

$$E \text{ vs. SHE} = -0.127 - 0.059 \times \lg[X^-] = 0.116 \text{ V} \quad (9)$$

The calculation results showed that when the SIBX concentration was 7.5×10^{-5} mol/L, the oxidation potential of the SIBX on the surface of pyrite was 0.116 V. The oxidation of X^- into X_2 occurred preferentially, and the potential formed by X_2 was the starting potential of flotation [29]. As can be seen in Fig. 10(a), the flotation slurry potential is higher than the minimum oxidation potential value required for oxidation of pyrites, and the pyrites are electrochemically adsorbed on the surface of pyrite. Pyrite surface oxidation affects the electric double layer charge density and affects the electrochemical adsorption of the collector on its hydrophobic surface.

Zeta potential analysis was carried out for pyrite at different altitude. As can be seen in Fig. 10(b), the isoelectric point (IEP) of pyrite was 5.3 at high altitude, while it was 6.2 at low altitude, which is consistent with the IEP of the oxidized pyrite surface [30–31]. The pyrite surface oxidation was formed as Fe–OH, where the IEP of $Fe(OH)_3$ were between 5.2 and 8.6 [24]. The oxidation of pyrite surface slows down at high altitude due to lower DO, and the Fe^{3+} content and Eh in the slurry was lower. In addition, it was also known from XPS analysis that more S_n^{2-}/S^0 is produced on the surface of pyrite in the low DO, some of which may be adsorbed on the surface of pyrite as thiosulfate or sulfite, resulting in lower IEP at the high altitude [24,32–33]. SIBX is the most traditional anionic collector agent for sulfide ore, and its addition will reduce the IEP of sulfide ore. The magnitude of zeta potential shift at high altitude is significantly larger than that of low altitude, which can explain to some extent that pyrite will adsorb more agents at high altitude. At the same time, excessive oxidation of the pyrite surface can be detrimental to agent adsorption at low altitudes.

3.3.4. FT-IR and UV-vis analysis

The FT-IR absorption spectra is used to analyze the mechanism of flotation agent–mineral interaction. In addition, to quantitatively identify the adsorption of SIBX on the surface of pyrite, UV-vis absorption analysis was used to determine the quantity of SIBX in the flotation slurry.

As can be seen in Fig. 11(a), the peaks at 2969.5 and 2875.0 cm^{-1} are caused by the stretching vibration of C–H in methyl and isomethyl, respectively; the peak at 1613.5 and 1468.8 cm^{-1} is caused by the stretching vibration of C=O in amide or by the stretching vibration of C=C and the antisymmetric deformation vibration of $–CH_3$ or the deformation vibration of $–CH_2$, respectively; the peaks at 1242.2, 1127.4, 1048.4, and 979.2 cm^{-1} is caused by the bending vibration of –C–O–C–, stretching vibration of –C–O–C–, stretching vibration of C=S, and bending vibration of C–H, respectively [9,34–38].

Comparing the FT-IR spectra of pyrite, the FT-IR spectra of pyrite after absorption of SIBX at different altitude are similar (Fig. 11(b)). The appeared absorption peaks at 1242.2 and 980.8 cm^{-1} are assigned to –C–O–C– and C–H, respectively, and no obvious C=S peaks are detected. It has been shown that the characteristic peak at 1242 cm^{-1} is ascribed to

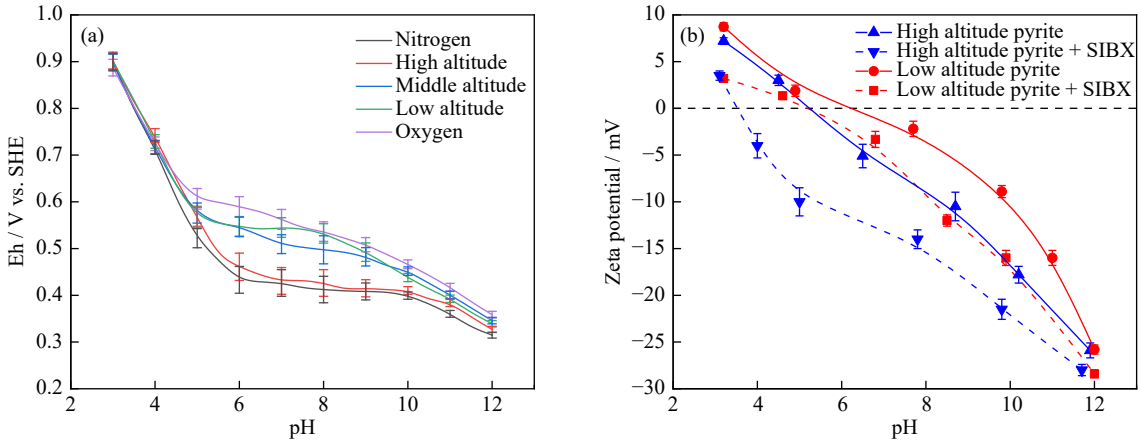

Fig. 10. (a) Eh and (b) Zeta potential of flotation slurry at different pH.

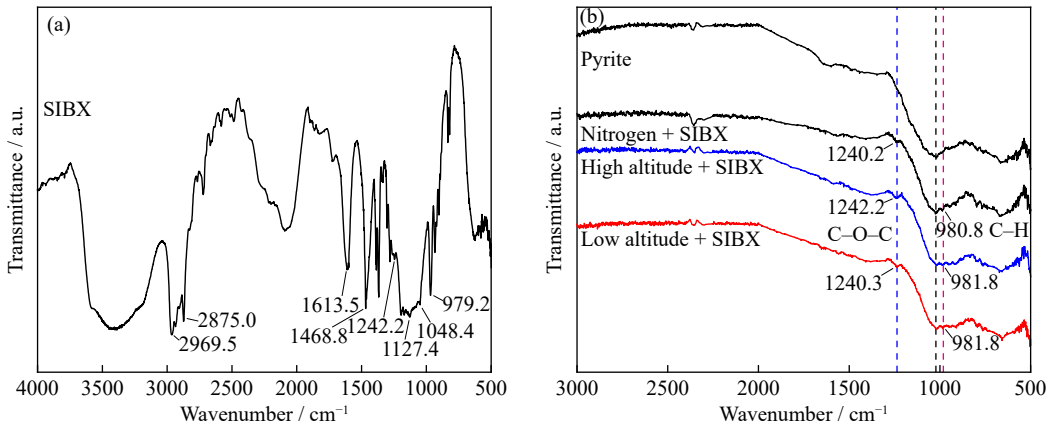

Fig. 11. FT-IR spectra of (a) SIBXand (b) adsorption at different altitudes.

–C–O–C– stretching vibration [39], which can be used as a dixanthogen characteristic peak to some extent. The formation of dixanthogen is more important for the flotation of pyrite than iron-xanthate [34]. FT-IR results show that the degree of oxidation of pyrite has no effect on the adsorption form of SIBX, it was able to adsorb on its surface and produce a dixanthogen adsorption layer. The characteristic peak of pyrite adsorption is weaker in the condition of nitrogen than in the case of oxygen, and DO has an effect on the quantity of pyrite agent adsorption, for which UV-vis absorption analysis was performed.

A series of standard solutions with concentrations of 0, 0.25×10^{-4}, 0.5×10^{-4}, 0.75×10^{-4}, and 1.0×10^{-4} mol/L were configured, and the absorbance of the solutions was measured at the characteristic absorption wavelength of 301 nm of SIBX to make the absorbance standard curve of the agent [40–42]. The SIBX standard line and the adsorption curve of the agent are shown in Figs. 12–13.

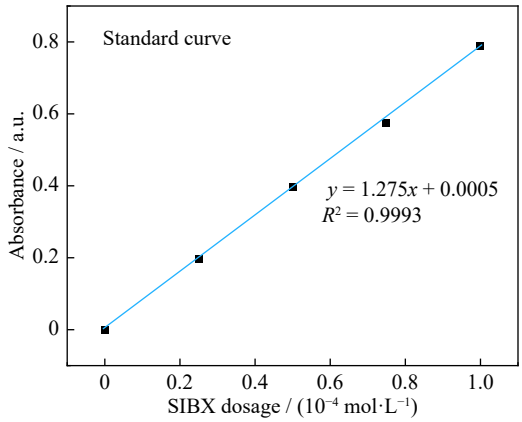

Fig. 12. SIBX concentration standard curve.

The R^2 of the standard line of SIBX concentration is good, and the absorbance and the concentration of the agent followed Beer's law [43]. The adsorption of SIBX on pyrite increases with increasing SIBX concentration, and the growth trend is gradually decreasing. The adsorption quantity was maximum at high altitude conditions, and it was greater at low altitude than that at nitrogen conditions, and moderate oxidation was favorable to the adsorption of SIBX on the surface of pyrite. Although the DO is lower in high altitude conditions, the oxygen mass transfer is sufficient to allow the oxidation of pyrite to provide sufficient adsorption sites on the surface.

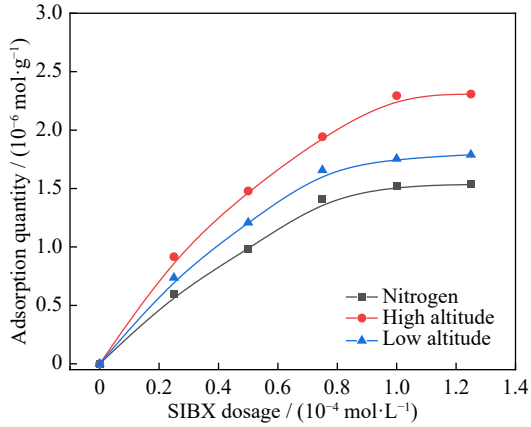

Fig. 13. SIBX content on pyrite.

3.3.5. AFM analysis

The contact angle and XPS analysis show that the oxidation rate of pyrite surface slows down at high altitude with low DO conditions, producing more S_n^{2-}/S^0 and enhanced surface hydrophobicity. The presence of S^0 reduces the adsorption sites of agents on the surface of pyrite, but electrochemical analysis, FT-IR, and UV-vis absorption analysis indicate that the adsorption of xanthate/dixanthogen occurs at different altitude conditions, and the adsorption is greatest under high altitude conditions. Therefore, AFM was used to study the adsorption morphology of the agent on the surface of pyrite at different altitude conditions and to analyze the interaction mechanism between SIBX and pyrite surface from the microscopic.

Fig. 14 shows the adsorption morphology of SIBX on the surface of pyrite at different altitude with a scan range of 3 μm × 3 μm. In the condition of nitrogen, SIBX was adsorbed on the surface of pyrite in a dotted form with a peak of up to 6 nm and a small amount of adsorption. Although pure nitrogen was used to repel oxygen from the slurry, the slurry was not completely in a dissolved oxygen-free state (DO < 0.3 mg/L), and oxygen mass transfer behavior still existed, and the oxidation of pyrite was slowed down. If oxidation produces charge transfer, smaller adsorption sites on the pyr-

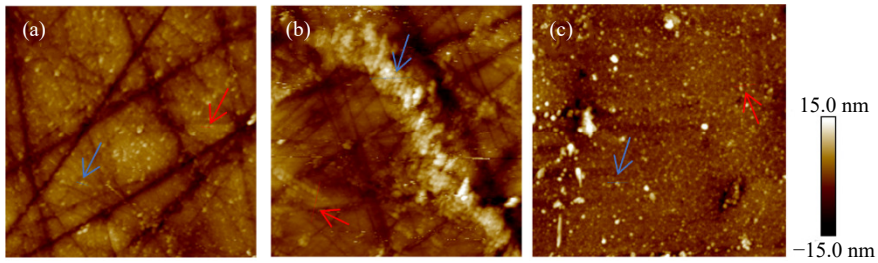

Fig. 14. 2D images of SIBX adsorption on pyrite surface at different altitude: (a) nitrogen; (b) high altitude; (c) low altitude.

ite surface will still be possible in relatively dispersed areas. The extensive adsorption of xanthate supports the model of Valdivieso [30], which suggests that the unoxidized sites can serve as initial nucleation sites for the formation of dixanthogen clusters.

As can be seen in Fig. 15, SIBX adsorbs on pyrite surfaces in block/columnar form and forms multiple lattice adsorption structures, with less cluster adsorption at high altitudes. The peak reaches up to 12 nm and the width exceeds 200 nm. Mermillod-Blondin proposed a xanthate adsorption mechanism in which these columnar oxidation structures are introduced [44], in which the xanthate preferentially interacts near the top of these oxidation structures, leading to the release of the underlying iron ion sites and the xanthate is adsorbed as a monolayer iron-xanthate followed by multilayered dixanthogen clusters.

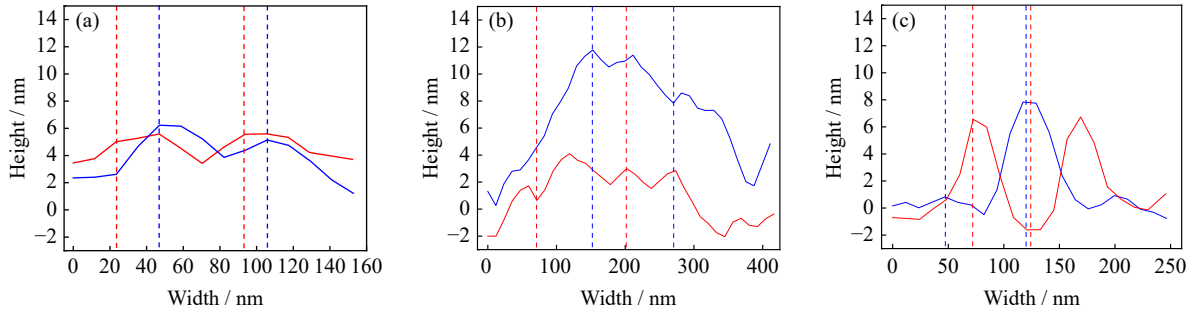

Fig. 15. SIBX adsorption layer height at the scribed line: (a) nitrogen; (b) high altitude; (c) low altitude.

At low altitude, due to the high DO, the pyrite surface is oxidized vigorously and more cavity corrosion areas appear, and it is difficult for SIBX to appear as a massive/columnar adsorption layer. However, cluster/spot adsorption morphology can still be found as shown in Fig. 15(c). The average peak height of these patches is 7 nm, and the maximum peak height can reach 12 nm. The oxygen mass transfer efficiency is higher at low altitude, and the oxidation behavior of pyrite surface is obvious and the charge distribution is more uniform, resulting in the adsorption sites uniformly dispersed on the pyrite surface in clusters/spots. However, the increase of Fe–OH may prevent the adsorption of xanthate on the clusters, and the massive oxidation of defective sulfur can destroy the original hydrophobicity, which explains the results of the XPS analysis and the contact angle test.

In summary, the main compounds adsorbed by SIBX on the surface of pyrite are dixanthogen and iron-xanthate [34]. The adsorption behavior of the collector agent relies mainly on electrochemical adsorption, but the unoxidized sites are equally likely to have dixanthogen adsorption. The adsorption of SIBX is weak under nitrogen conditions due to the low surface potential. Oxidative corrosion exists at low altitude conditions and the adsorption of the agent is carried out in clusters/spots on the surface of pyrite. The best adsorption effect of the SIBX under high altitude conditions was carried out in block/column form and formed multiple lattice adsorption structures. This reveals the main reason for the maximum adsorption of the agent in pyrite at high altitude.

4. Conclusions

Under atmospheric pressure conditions and high-altitude, low-oxygen atmosphere was simulated by adjusting the oxygen partial pressure and measuring dissolved oxygen in water. Pyrite flotation tests and mechanistic studies were conducted under these conditions with the following conclusions:

(1) The pyrite flotation tests indicate that pyrite flotation requires moderate oxidation and neither nitrogen/oxygen atmosphere is conducive to pyrite recovery. Compared with the conventional low altitude system, the high altitude low dissolved oxygen is favorable for pyrite flotation but unfavorable for suppression.

(2) Pyrite hydrophobicity is influenced by the presence of surface S_n^{2-}/S^0 or hydroxyl iron. XPS analysis shows that the presence of a large number of sulfur defect sites and relatively small amounts of SO_4^{2-} and Fe(III)–O/OH components on the surface of pyrite at high altitude atmospheres enhances the interaction of pyrite with SIBX along with hydrophobicity. The contact angle also corroborates the conclusion.

(3) SIBX was used as a collector, and after electrochemical calculations, the test atmospheres met the minimum requirement of dixanthogen oxidation potential. FT-IR analys-

is shows that there was dixanthogen adsorption peak on the surface of pyrite, and the floatability of pyrite was influenced by the adsorption quantity. Zeta potential and UV-vis absorption analysis indicate that the high altitude conditions were favorable for SIBX adsorption. AFM analysis exhibits SIBX was stably adsorbed on the surface of pyrite in a lattice structure consisting of columns/blocks under high altitude.

(4) In this thesis, the oxidation of pyrite surface and adsorption behavior of collector were investigated under low dissolved oxygen conditions at high altitude. The findings are consistent with the oxidation mechanism of pyrite and the electrochemical theory of sulfide ore flotation. They show a systematic description of sulfide ore flotation under low dissolved oxygen, providing a theoretical basis for sulfide ore flotation under high altitude conditions.

(5) Xanthate–collector can be generalized due to the consistency of the polar groups. However, we need to study more systematically whether other types of agents (e.g., ethyl sulfide or beneficiation black powder, etc.) also satisfy this adsorption model.

Acknowledgements

The research of was supported by of the National Key Research and Development Program of China (No. 2022YFC 2904601), and the flotation test of pyrite was mainly done by Guangke Ye.

Conflict of Interest

The authors declare that they have no known competing financial interests or personal relationships that could have appeared to influence the work reported in this paper.

References

[1] S.C. Lu, Advances in flotation theory for sulphide ores, *Metallic Ore Dressing Abroad*, (1974), No. 6, p. 30.

[2] N. Arbiter, C.C. Harris, and R.F. Yap, The air flow number in flotation machine scale-up, *Int. J. Miner. Process.*, 3(1976), No. 3, p. 257.

[3] X.P. Niu, *Correlation of Surface Oxidation of Galena, Chalcopyrite and Pyrite with Their Floatability* [Dissertation], University of Chinese Academy of Sciences, Beijing, 2019, p. 70.

[4] H.P. Zhao, X.P. Niu, B.X. Dong, X.B. Jia, and R.M. Ruan, Investigation on the correlation between ferrous ion and the floatability of pyrite with different oxidation degrees, *Miner. Eng.*, 184(2022), art. No. 107636.

[5] T. Hirajima, H. Miki, G.P.W. Suyantara, *et al*., Selective flotation of chalcopyrite and molybdenite with H_2O_2 oxidation, *Miner. Eng.*, 100(2017), p. 83.

[6] A. Mazumdar, T. Goldberg, and H. Strauss, Abiotic oxidation of pyrite by Fe(III) in acidic media and its implications for sulfur isotope measurements of lattice-bound sulfate in sediments, *Chem. Geol.*, 253(2008), No. 1-2, p. 30.

[7] J.R. Mycroft, H.W. Nesbitt, and A.R. Pratt, X-ray photoelectron and Auger electron spectroscopy of air-oxidized pyrrhotite: Distribution of oxidized species with depth, *Geochim. Cosmochim. Acta*, 59(1995), No. 4, p. 721.

[8] Y.C. Liu, Y.Q. Li, J.H. Chen, D. Kang, and X. Yang, Influence of sulfur vacancy on pyrite oxidization by water and oxygen molecules, *Colloids Surf. A*, 634(2022), art. No. 127954.

[9] M.B.M. Monte, F.F. Lins, and J.F. Oliveira, Selective flotation of gold from pyrite under oxidizing conditions, *Int. J. Miner. Process.*, 51(1997), No. 1-4, p. 255.

[10] W.Z. Yin, J.W. Xue, D. Li, Q.Y. Sun, J. Yao, and S. Huang, Flotation of heavily oxidized pyrite in the presence of fine digenite particles, *Miner. Eng.*, 115(2018), p. 142.

[11] S.M. Bulatovic, *Handbook of Flotation Reagents*, Amsterdam: Elsevier, (2007), p. 235.

[12] C.J. Martin, S.R. Rao, J.A. Finch, and M. Leroux, Complex sulphide ore processing with pyrite flotation by nitrogen, *Int. J. Miner. Process.*, 26(1989), No. 1-2, p. 95.

[13] S. Aghazadeh, S.K. Mousavinezhad, and M. Gharabaghi, Chemical and colloidal aspects of collectorless flotation behavior of sulfide and non-sulfide minerals, *Adv. Colloid Interface Sci.*, 225(2015), p. 203.

[14] W.Q. Qin, X.J. Wang, L.Y. Ma, *et al*., Electrochemical characteristics and collectorless flotation behavior of galena: With and without the presence of pyrite, *Miner. Eng.*, 74(2015), p. 99.

[15] W.J. Zhang, X. Jin, Z.T. Feng, *et al*., Collectorless flotation separation of molybdenite from complex sulfide minerals employing a bi-carbonyl depressant, *Sep. Purif. Technol.*, 322(2023), art. No. 124207.

[16] D.W. Clark, A.J.H. Newell, G.F. Chilman, and P.G. Capps, Improving flotation recovery of copper sulphides by nitrogen gas and sulphidisation conditioning, *Miner. Eng.*, 13(2000), No. 12, p. 1197.

[17] B. Wiencke, A proposed new model for the prediction of latitude-dependent atmospheric pressures at altitude, *Sci. Technol. Built Environ.*, 27(2021), No. 9, p. 1221.

[18] R.M. Rosenberg and W.L. Peticolas, Henry's law: A retrospective, *J. Chem. Educ.*, 81(2004), No. 11, art. No. 1647.

[19] R. Sander, Compilation of Henry's law constants (version 4.0) for water as solvent, *Atmos. Chem. Phys.*, 15(2015), No. 8, p. 4399.

[20] K. Jiang, Y.X. Han, J. Liu, Y. Wang, W.C. Ge, and D.J. Zhang, Experimental and theoretical study of the effect of pH level on the surface properties and floatability of pyrite, *Appl. Surf. Sci.*, 615(2023), art. No. 156350.

[21] Y.F. Mu, Y.P. Cheng, and Y.J. Peng, The interaction of grinding media and collector in pyrite flotation at alkaline pH, *Miner. Eng.*, 152(2020), art. No. 106344.

[22] N. Nirmalkar, A.W. Pacek, and M. Barigou, On the existence and stability of bulk nanobubbles, *Langmuir*, 34(2018), No. 37, p. 10964.

[23] N. Anton, P. Pierrat, G.A. Brou, *et al*., The pH-induced specific area changes of unsaturated lipids deposited onto a bubble interface, *Langmuir*, 37(2021), No. 8, p. 2586.

[24] P. Forson, M. Zanin, W. Skinner, and R. Asamoah, Differential flotation of pyrite and Arsenopyrite: Effect of pulp aeration and the critical importance of collector concentration, *Miner. Eng.*, 178(2022), art. No. 107421.

[25] S.H. Xu, M. Zanin, W. Skinner, and S. Brito e Abreu, Surface chemistry of oxidised pyrite during grinding: ToF-SIMS and XPS surface analysis, *Miner. Eng.*, 170(2021), art. No. 106992.

[26] D.Z. Liu, G.F. Zhang, and B.B. Li, Electrochemical and XPS investigations on the galvanic interaction between pentlandite and pyrrhotite in collectorless flotation system, *Miner. Eng.*, 190(2022), art. No. 107916.

[27] S. Mattila, J.A. Leiro, and M. Heinonen, XPS study of the oxidized pyrite surface, *Surf. Sci.*, 566-568(2004), p. 1097.

[28] Y.F. Cai, Y.G. Pan, J.Y. Xue, Q.F. Sun, G.Z. Su, and X. Li, Comparative XPS study between experimentally and naturally weathered pyrites, *Appl. Surf. Sci.*, 255(2009), No. 21, p. 8750.

[29] W. Chimonyo, K.C. Corin, J.G. Wiese, and C.T. O'Connor, Redox potential control during flotation of a sulphide mineral

ore, *Miner. Eng.*, 110(2017), p. 57.
[30] A.L. Valdivieso, A.A.S. López, and S. Song, On the cathodic reaction coupled with the oxidation of xanthates at the pyrite/aqueous solution interface, *Int. J. Miner. Process.*, 77(2005), No. 3, p. 154.
[31] A.L. Valdivieso, T.C. Cervantes, S. Song, A.R. Cabrera, and J.S. Laskowski, Dextrin as a non-toxic depressant for pyrite in flotation with xanthates as collector, *Miner. Eng.*, 17(2004), No. 9, p. 1001.
[32] R.S. Multani, H. Williams, B. Johnson, R.H. Li, and K.E. Waters, The effect of superstructure on the zeta potential, xanthate adsorption, and flotation response of pyrrhotite, *Colloids Surf. A*, 551(2018), p. 108.
[33] S. Zhang, Y.J. Xian, S.M. Wen, G.Y. Liang, and Q. Geng, Contribution of ammonia in xanthates adsorption onto copper oxide mineral surface in high-alkaline solution, *Appl. Surf. Sci.*, 630(2023), art. No. 157294.
[34] Y.H. Zhang, Z. Cao, Y.D. Cao, and C.Y. Sun, FTIR studies of xanthate adsorption on chalcopyrite, pentlandite and pyrite surfaces, *J. Mol. Struct.*, 1048(2013), p. 434.
[35] G. Bulut and S. Atak, Role of dixanthogen on pyrite flotation: Solubility, adsorption studies and Eh, FTIR measurements, *Min. Metall. Explor.*, 19(2002), No. 2, p. 81.
[36] J. Yu, Y.Y. Ge, and X.W. Cai, The desulfurization of magnetite ore by flotation with a mixture of xanthate and dixanthogen, *Minerals*, 6(2016), No. 3, art. No. 70.
[37] Y. Ma, M. Yang, L. Tang, *et al*., Flotation separation mechanism for secondary copper sulfide minerals and pyrite using novel collector ethyl isobutyl xanthogenic acetate, *Colloids Surf. A*, 634(2022), art. No. 128010.
[38] J. Wu, B.Q. Yang, R. Martin, *et al*., Anisotropic adsorption of xanthate species on molybdenite faces and edges and its implication on the flotation of molybdenite fines, *Miner. Eng.*, 207(2024), art. No. 108571.
[39] Q. Zhang, Y.H. Hu, G.H. Gu,and Z.H. Nie, Electrochemical flotation of ethyl xanthate-pyrrhotite system, *Trans. Nonferrous Met. Soc. China*, 14(2004), No. 6, p. 1174.
[40] R. Woods, C.I. Basilio, D.S. Kim, and R.H. Yoon, Ethyl xanthate chemisorption isotherms and Eh-pH diagrams for the silver+water+ethyl xanthate system, *J. Electroanal. Chem.*, 328(1992), No. 1-2, p. 179.
[41] S. Zhang, Y.J. Xian, S.M. Wen, and G.Y. Liang, Enhancement of xanthate adsorption on lead-modified and sulfurized smithsonite surface in the presence of ammonia, *Miner. Eng.*, 189(2022), art. No. 107872.
[42] Y.H. Zhang, L.M. Wu, P.P. Huang, Q. Shen, and Z.X. Sun, Determination and application of the solubility product of metal xanthate in mineral flotation and heavy metal removal in wastewater treatment, *Miner. Eng.*, 127(2018), p. 67.
[43] T.G. Mayerhöfer and J. Popp, Beer's law derived from electromagnetic theory, *Spectrochim. Acta Part A*, 215(2019), p. 345.
[44] R. Mermillod-Blondin, M. Kongolo, P. De Donato, *et al.*, Pyrite flotation with Xanthate under alkaline conditions-Application to environmental desulfurisation, [in] *Centenary of Flotation Symposium*, Brisbane, 2005, p. 683.